Secondary instabilities in shock-induced transition to turbulence

P. Vorobieff[1,2], C. Tomkins[2], S. Kumar[2], C. Goodenough[2], N.-G. Mohamed[1] & R. F. Benjamin[2]
[1]*The University of New Mexico, Albuquerque, New Mexico, USA*
[2]*Los Alamos National Laboratory, Los Alamos, New Mexico, USA*

Abstract

Richtmyer-Meshkov instability (RMI) occurs wherever a density gradient is impulsively accelerated, e.g., by a shock wave. Misalignment between pressure and density gradients leads to baroclinic production of vorticity, the latter resulting in formation of vortical structures after the shock wave passage. The vortex-dominated evolution of the flow eventually leads to turbulence. In the process of RMI-induced transition to turbulence, several secondary instabilities could develop in the flow, driven, e.g., by shear (Kelvin-Helmholtz) or by density-pressure gradient misalignment (secondary baroclinic instability). The exact nature of the secondary instabilities has been the subject of some discussion in the literature, with different authors observing shear-induced and baroclinic secondary instabilities. To resolve the issue, we have undertaken an experimental study of a Mach 1.2 shock-accelerated column of heavy gas (sulfur hexafluoride) immersed in a lighter gas (air). For visualization and quantitative analysis purposes, we use planar laser-induced fluorescence of acetone tracer pre-mixed with the heavy gas, which makes it possible to resolve the small-scale (down to 12 microns) structure of the flow. Our observations of the RMI-driven flow around the gas column show the presence of two apparently distinct secondary instabilities: instability inside the vortex cores as well as the instability along the outer edge of the primary vortex spirals of the heavy gas. The former is consistent with the reports of baroclinic instability, while the latter is likely shear-induced.
Keywords: Richtmyer-Meshkov instability, hydrodynamics, flow visualization.

Advances in Fluid Mechanics V, A. Mendes, M. Rahman & C. A. Brebbia (Editors)

1 Introduction

There are several reasons why Richtmyer-Meshkov instability (RMI) attracted considerable attention from researchers in recent years, although it was predicted theoretically by Richtmyer [1] in the late 1950s and demonstrated experimentally by Meshkov [2] about a decade later. The mechanism that drives the instability is baroclinic production of vorticity ω that can be represented by the vorticity equation with the diffusive terms dropped:

$$\frac{D}{Dt}\left(\frac{\omega}{\rho}\right) = \frac{1}{\rho^3}\nabla\rho \times \nabla p \tag{1}$$

In Eq. 1, D/Dt is the convective derivative. New vorticity is produced wherever the cross-product of the gradients of pressure p and density ρ is non-zero. Thus a passage of a shock wave through a sharp or diffuse interface between two fluids of different density would lead to vorticity deposition on the interface. This happens both when the shock travels from the heavier fluid into the lighter fluid and when it traverses the density interface in the opposite direction. This is an important difference between RMI and the gravity-driven baroclinic Rayleigh-Taylor instability (RTI), which develops only in the case when the initial stratification of the fluid in a gravity field is unstable (heavy fluid above light fluid). Another difference between RMI and RTI is the way energy is supplied to the instability. In the case of RTI, the energy is supplied continuously, while RMI is triggered by a limited amount of energy in the interval when the pressure gradient (shock) traverses the interface. In this context, the name of RMI has often been applied to any impulsively-driven density interface instability [1, 3].

The recent interest to RMI can be explained by a combination of three factors. First, it is important in a variety of problems - from supernova explosion [4] to scramjet engine design [5]. Second, RMI-driven flows now serve as an important numerical code validation benchmark [6, 7]. RMI-driven codes serve as a convenient quantitative benchmark because the initial conditions of the flow can be characterized in detail experimentally, the energy input into the flow is known and finite, and subsequent measurements can provide specific quantitative information about the flow evolution. For the numerics to faithfully reproduce an experimental RMI benchmark, the code must have good models for compressibility effects, for mixing, and for the dynamics of vortex-driven flows. Finally, the studies of RMI-induced transition to turbulence [8, 9, 10] use the same features that make RMI-driven flows good for benchmarking (i.e., explicit knowledge of initial conditions and finite energy input) to provide insight into the general problem of transition to turbulence and emergence of disordered flow features from a vortex-driven, predominantly deterministic early-time flow.

Transition to turbulence in an RMI-driven mixing flow can be described thus. Initial vorticity deposition occurs within a very short period compared with the time it takes for the flow to become turbulent. The vorticity field forms on the density interface after the shock passage (or impulsive acceleration). After a short interval of linear growth, when the amplitude of the interfacial perturbations grows

Advances in Fluid Mechanics V, A. Mendes, M. Rahman & C. A. Brebbia (Editors)

Figure 1: A sequence of images showing the evolution of a Mach 1.2 shock-accelerated cylinder of sulfur hexafluoride embedded in air. The flow direction is from left to right. The images were produced by illuminating a planar section of the flow (normal to the axis of the cylinder) with a pulsed laser sheet. The first image represents the initial conditions immediately before the shock arrival (cylinder diameter 3 mm). The timing of the subsequent images is 60, 200, 340, 480, 620, 760, and 1300 μs after the shock acceleration. The physical vertical extent of the imaged area is 18.5 mm.

in agreement with the original theory of Richtmyer [1], the flow enters the stage of deterministic, vortex-dominated nonlinear growth. The perturbation amplitude evolution at this stage is well described by recent theory [11, 12]. At some time during this stage, secondary instabilities begin to develop in the flow. Experimental measurements of the velocity field [10, 13] show strong shear present in the flow at the vortex-dominated stage, suggesting a possibility of shear-driven secondary instability (Kelvin-Helmholtz). At the same time, advection of material of different density into the vortex cores could again lead to baroclinic vorticity production due to centripetal acceleration associated with rotation. Baroclinic secondary instability in the vortex cores under these circumstances has been reported in numerical simulations [7]. The emergence of secondary instabilities adds a disordered element to the flow and initiates transition to turbulence, with evidence of a turbulent cascade developing in the velocity field scaling [13].

In this paper, we report results from an experimental study of RMI-induced transition to turbulence in a shock-accelerated cylinder of heavy gas (SF_6) embedded in lighter gas (air), as shown in Fig. 1. Our study concentrates on the identification of secondary instabilities leading to turbulent transition. The experimental technique we employ (flow visualization via laser-induced fluorescence, or LIF) makes it possible to resolve the fine structure of the flow in unprecedented detail. The new data acquired with this technique show evidence that both baroclinic and shear-driven secondary instabilities play a role in the transition of the shock-accelerated mixing flow to turbulence.

2 Experimental setup and diagnostics

Earlier experiments with shock-accelerated gas curtains [8, 9, 10] and gas cylinders [14] employed laser-sheet visualization, with a section of the flow illuminated by a laser sheet produced by passing a laser beam through a combination of a spherical and a cylindrical lens. The heavy gas (SF_6) was pre-mixed with submicron-sized

Advances in Fluid Mechanics V, A. Mendes, M. Rahman & C. A. Brebbia (Editors)

droplets of glycol. Light scattered from these droplets was recorded with a digital camera as mixing and eventually transition to turbulence took place in the shock-accelerated flow (Fig. 1). Glycol droplets as tracers have several important advantages. Signal sufficient for effective visualization can be recovered from the flow illuminated with a relatively low-powered visible-light laser. Also, with high resolution images spaced closely enough in time, it is possible to track the movement of droplets from image to image and thus reconstruct the instantaneous velocity field via particle image velocimetry (PIV) [10, 13]. However, investigation of mixing on the small scales in the flow, which is essential for the understanding of the secondary instability mechanisms, requires a resolution that the glycol tracer simply cannot provide. With a glycol droplet size on the order of 0.5 μm and approximately one droplet in each cubic volume of SF_6 10 μm on the side, the minimal size of a flow structure that can be successfully resolved is between 20 and 100 μm. Thus a decision was made to switch from tracer in the form of vapor droplets to tracer gas.

For the visualization of the experiment, we originally employed a New Wave Technology Nd:YAG Gemini PIV 200 laser, capable of producing short-duration (5 ns), powerful (up to 200 mJ) pulses of coherent light. Presence of two optical heads and excellent timing controllability make this laser an excellent choice for visualization of high-speed fluid flows. The laser was specifically developed for PIV measurements. The laser was supplied in the frequency-doubled configuration, with a wavelength of 532 nm (green).

Our new challenge lay in adapting the laser to LIF, which is a considerably different kind of diagnostic. LIF uses tracer gas that, when illuminated with coherent light, emits fluorescence with a wavelength distinct from that of the incident light. Among fluorescent gases are biacetyl, acetone and iodine. Biacetyl was successfully employed in some early RMI studies, but was not deemed an appropriate choice because of its strong and unpleasant smell. After preliminary experiments with iodine produced unsatisfactory results, we decided on acetone as the tracer gas of choice. Use of acetone required a modification to the laser, namely frequency-quadrupling to wavelength 266 nm. After the modification, further development of the LIF diagnostic for high-speed flows took place at the DX-3 gas shock tube (see Ref. [14] for a detailed description of the facility) in Los Alamos National Laboratory.

In the shock tube experiments, the initial conditions were formed by a gravity feed supplying sulfur hexafluoride (SF_6) into the test section of the shock tube through a circular nozzle. The modular setup of the test section facilitated quick replacement of the nozzles to produce gas cylinders of different diameters (3 to 8 mm). The shock tube had a 75-mm square cross section, with optical windows in the test section for visualization (Fig. 2), and with an optical window at the downstream end for the laser sheet illumination. In some of the experiments described here, the camera was positioned not above the test section as shown in Fig. 2, but underneath it. The Mach 1.2 planar shock wave propagating through the test section was formed by pressurizing a driver section ($\sim$ 2.5m upstream of the test section) and then puncturing the diaphragm separating the driver section from the

Advances in Fluid Mechanics V, A. Mendes, M. Rahman & C. A. Brebbia (Editors)

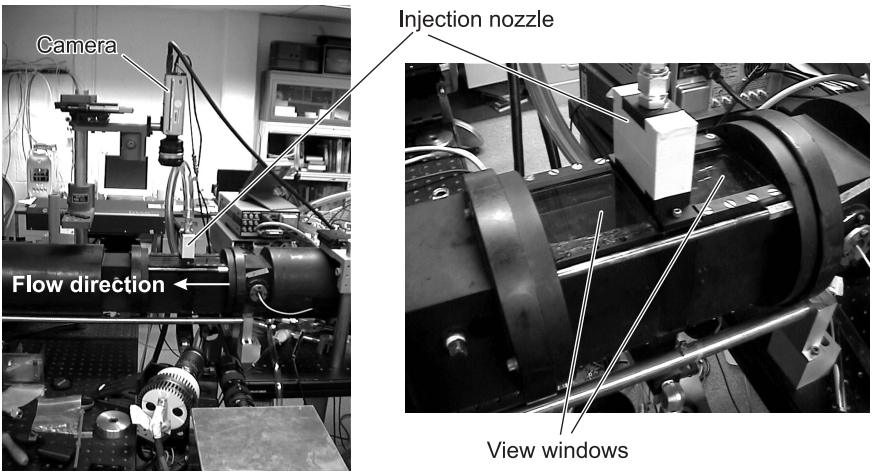

Figure 2: The shock tube: left – general view, right – close-up of the test section.

rest of the shock tube. After the initial shock acceleration (shock front velocity 400 m/s), the mean (piston) velocity of the flow was close to 100 m/s. During the tests, sulfur hexafluoride was pre-mixed with saturated acetone vapor and imaged with an Apogee cooled-CCD camera. The mix was produced by bubbling SF_6 through liquid acetone. We sought to produce a quantitative interpretation of the imaged flow fields in terms of the volume fraction of the SF6+tracer mix. This involved resolving several calibration issues. First, we had to determine that our acetone vapor was saturated. This was achieved by variation of the distance traveled by the SF6 bubbles through the mixing apparatus with simultaneous measurements of the fluorescence in the mix. Second, we had to determine the rate of fluorescence decay in the light sheet due to absorption. The decay turned out to be exponential, in good agreement with theory. Third, the influences of the CCD properties and the CCD camera lens properties had to be calibrated out. The cooled, high-sensitivity 1024 by 1024 pixel CCD (Apogee) we used to record our images had a relatively stable dark field (worst-case variation of intensity less than 1%), so twelve images of the dark field were taken, ensemble-averaged and subtracted from the experimental images. Images of a uniformly illuminated flat field were taken and, after dark field subtraction, analyzed to determine any intensity non-uniformity due to vignetting (lens-induced decrease of intensity near the corners). Ensemble averaging of the flat field produced an intensity calibration map to remove the vignetting effect. Finally, prior to every change in the optical setup producing the light sheet, we took images of the test section of the shock tube uniformly filled with the SF_6+acetone mix. This was done to double-check the fluorescence decay rate (and eliminate the possibility of acetone breakdown due to excess illumination) and to assess the non-uniformity of the intensity of the light sheet (roughly Gaussian fall-off towards the edges).

Advances in Fluid Mechanics V, A. Mendes, M. Rahman & C. A. Brebbia (Editors)

After all these measures were implemented, we produced images resolving several thousand intensity levels at atmospheric pressure, with the laser pulse power maintained at $\sim$ 11 mJ/pulse and the spatial resolution of the images as high as 12 microns per pixel. This represents an approximately five-time improvement in resolution when compared with glycol-droplet tracer used in earlier experiments (where the effective resolution could be estimated as $\sim 60\ \mu$m).

3 Observations and analysis

In the case of a shock-accelerated gas cylinder, the general sequence of events leading to RMI-induced turbulent transition as described in the Introduction is depicted in Fig. 1. The density distribution in the initial conditions (first image to the left) is produced by injection of SF_6 into the test section through a circular nozzle, thus leading to a cylinder with a nearly circular cross-section and a diffuse interface between SF_6 and air. After shock acceleration, baroclinic deposition of vorticity (Eq. 1, Fig. 3) leads to roll-up of a pair of counter-rotating vortices that distort the initial density distribution by advecting the cylinder material into the vortex core (second through fourth images).

Formation of this large-scale structure of the flow is explained in Fig. 3. If the shock accelerates a small perturbation on a density interface, there are two possible cases for the perturbation amplitude growth. In the case shown in Fig. 3a, the shock goes from the lighter gas into the heavier gas. The amplitude of a small "bulge" of the heavy gas on the interface will start growing immediately after the shock acceleration due to the formation of two counter-rotating vortices on the sides of the "bulge." For a similar "bulge," but with the shock going from the heavy gas into the light gas (Fig. 3b), the baroclinic vorticity deposition will lead to the amplitude of the perturbation first decreasing and then beginning to grow again. The gas cylinder (Fig. 3c) can be schematically represented as a combination of the two initially perturbed interfaces shown in cases a and b. The perturbation amplitude on the upstream side starts growing immediately, whereas the downstream-side perturbation undergoes phase reversal, leading to the formation of a distinctive "mushroom-cap" shape advected by the two counter-rotating vortices. The second through fourth "mushroom-cap" images in Fig. 1 correspond to deterministic, vortex-dominated, nonlinear evolution of the instability. In this stage, the flow is largely two-dimensional, with apparently little change in the direction normal to the image plane in Fig. 1.

In subsequent images (fifth through seventh in Fig. 1), one can observe formation of small-scale perturbations, whose amplitude begins to grow. The secondary instability-induced perturbations are manifested by the small-scale sinuous distortion in the spirals of SF_6 formed by the advection into the cores of the vortices deposited by the initial RMI shock-cylinder interaction. Statistical analysis of the disordered flow field component associated with the secondary instabilities [13] suggests that the evolution of the secondary instabilities quickly leads to fully three-dimensional flow on the small scales. As time goes by, the role of the disordered flow features increases until at late times we observe a well-mixed flow

Advances in Fluid Mechanics V, A. Mendes, M. Rahman & C. A. Brebbia (Editors)

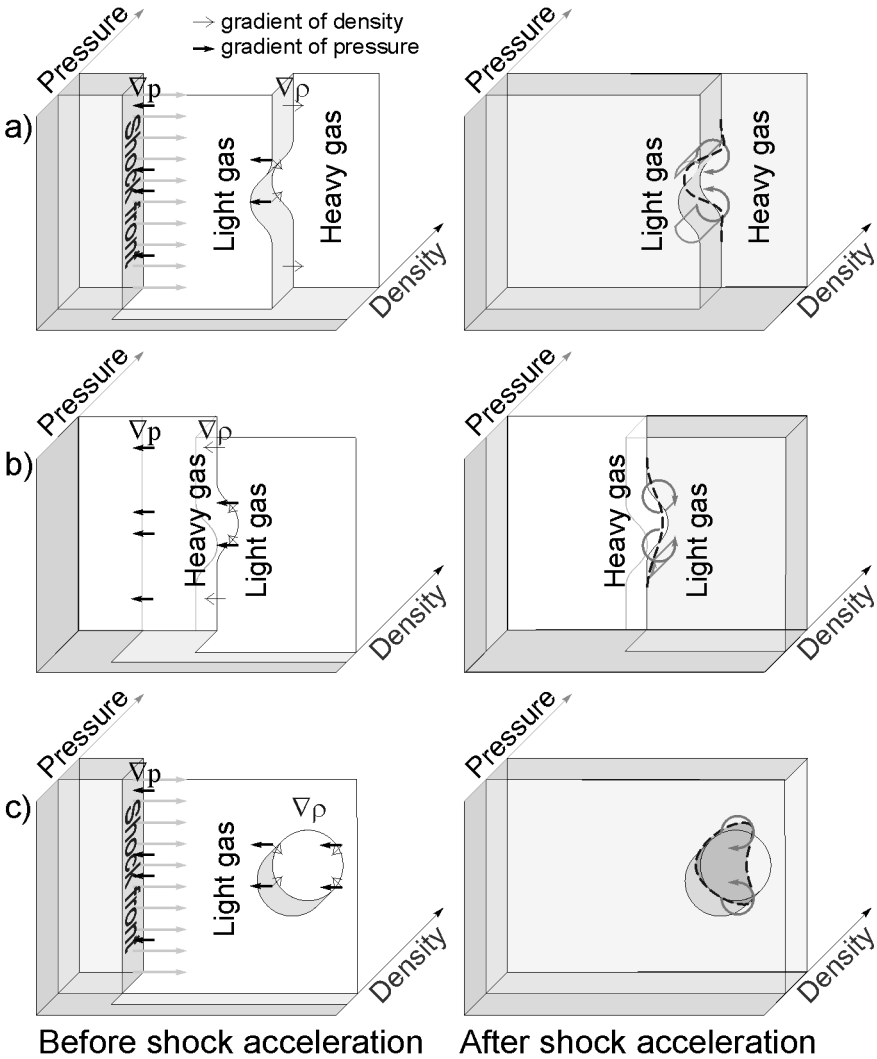

Figure 3: Schematic of RMI-driven evolution of a small perturbation on a light-to-heavy gas interface (a), on a heavy-to-light gas interface (b), and of the RMI-driven evolution of a cylindrical density interface (c). Left column represents the time before the shock acceleration of the interface, right column – the shock-accelerated interface.

with multiple scale present and the statistics approaching Kolmogorov turbulence (eighth image in Fig. 1).

Advances in Fluid Mechanics V, A. Mendes, M. Rahman & C. A. Brebbia (Editors)

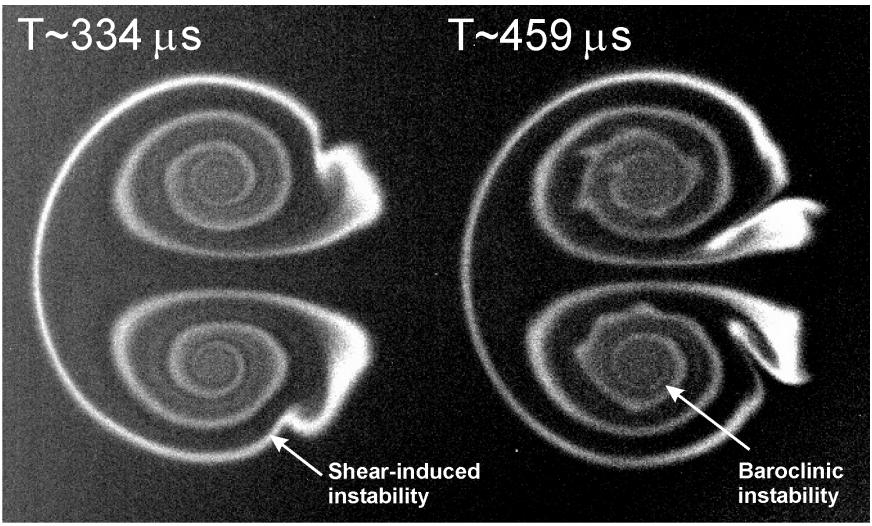

Figure 4: LIF visualization of the emergence of secondary instabilities in a shock-accelerated SF_6 cylinder pre-mixed with saturated acetone vapor. The vertical extent of the image area is 14 mm. Image resolution is 12 μm/pixel.

But where do the secondary instabilities form? Prior velocity measurements [13] show the presence of strong shear on the outer edges of the deformed cylinder, and this is where one could expect the instability onset if it is shear-driven. The strongest pressure gradient in the flow after the shock passage should be closer to the large-scale vortex cores, thus suggesting that the baroclinic secondary instability should form near these cores rather than on the periphery. The situation is complicated by the possibility that shear-induced perturbations can be advected into the vortex cores by the mean flow. Our earlier studies using PIV velocity measurements did show small-scale perturbations both on the periphery of the large-scale vortices and in the cores, but did not provide a definitive answer as to the origin of these perturbations.

Our recent images resolve the flow structure in sufficiently high detail in space and time to elucidate the matter. Figure 4 shows LIF visualization of two instances in the evolution of a shock-accelerated 3-mm initial diameter SF_6-acetone cylinder. The image was processed as described in the previous part to remove the effects of CCD dark-field non-uniformity and vignetting. For these initial conditions, the distance traveled by the laser light through the fluorescent medium would be too small to produce an appreciable decay due to absorption.

In this image, the two clearly visible large-scale vortices are produced by the initial shock interaction with the heavy-gas cylinder (as one can also observe in Fig. 1). The first exposure of the image (left) taking place 334 μs after the shock

Advances in Fluid Mechanics V, A. Mendes, M. Rahman & C. A. Brebbia (Editors)

shows formation of a perturbation on the periphery of the deforming gas cylinder, where one could expect the onset of shear-driven secondary instability. The second exposure, taken 125 μs later, shows the evolution of this perturbation, with some amplitude growth and propagation down the spiral. However, the second exposure clearly shows that the shear-induced instability has not propagated into the vortex core. Yet at the core we also observe a perturbation with a distinct characteristic wavelength and somewhat different morphology. This suggests that both the shear-driven and the baroclinic instability may play a role in RMI-induced transition to turbulence.

4 Conclusion

Our study of transition to turbulence initiated by impulsive acceleration of a density interface uses high-resolution flow visualization to produce images that provide insight into the role of secondary instabilities in the turbulent transition. The observations suggest that both baroclinic and shear-driven secondary instabilities play a role in the evolution of the disordered components of the flow whose emergence eventually leads to turbulence.

In the immediate future, these images will also be subjected to quantitative analysis to study the evolution of the mixing interface length (can a Liapunov exponent be extracted?), the concentration histogram history, the concentration structure function as the function of time, and other properties that may be relevant to the understanding of transition to turbulence in this problem, as well as the more general problem of turbulent transition. The same quantitative measurements will also serve as benchmarks for the validation of numerical codes.

Acknowledgments

This study was supported by the U.S. Department of Energy, Contract No. W-7405-ENG-36, and by the Defense Advanced Research Projects Agency (DARPA), grant NBCH1010004. The authors thank the Boeing Company for providing the University of New Mexico with funding for the visualization laser.

References

[1] Richtmyer, R.D., Taylor instability in shock acceleration of compressible fluids. *Communications on Pure and Applied Mathematics* **13**, pp. 297-319, 1960.

[2] Meshkov, E.E., Instability of the interface of two gases accelerated by a shock wave. *Izvestiya Akademii Nauk SSSR, Mekhanika Zhidkosti i Gaza* **4**, pp. 151-159, 1969.

[3] Niederhaus, C.E., and Jacobs, J.W., Experimental study of the Richtmyer-Meshkov instability of incompressible fluids. *Journal of Fluid Mechanics* **485**, pp. 243-277, 2003.

Advances in Fluid Mechanics V, A. Mendes, M. Rahman & C. A. Brebbia (Editors)

[4] Burrows, A., Hayes, J., and Fryxell, B.A., On the nature of core-collapse supernova explosions. *Astrophysics Journal* **450**, pp. 830-850, 1995.
[5] Yang,J., Kubota,T., and Zukoski, E.E., Applications of shock-induced mixing to supersonic combustion. *AIAA Journal* **31**, pp. 854-862, 1993.
[6] Baltrusaitis, R.M., Gittings, M.L., Weaver, R.P., Benjamin, R.F., and Budzinski, J.M., Simulation of shock-generated instabilities. *Physics of Fluids* **8**, pp. 2471-2483, 1996.
[7] Cook, A.W. and Zhou, Y., Energy transfer in Rayleigh-Taylor instability - art. no. 026312. *Physical Review E* **66**, pp. 026312-1 – 026312-12, 2002.
[8] Vorobieff, P., Rightley, P.M., and Benjamin, R.F., Power-law spectra of incipient gas-curtain turbulence. *Physical Review Letters* **81**, pp. 2240-2243, 1998.
[9] Vorobieff, P., Rightley, P.M., and Benjamin, R.F., Shock-driven gas curtain: fractal dimension evolution in transition to turbulence. *Physica D* **133**, pp. 469-476 (1999).
[10] Prestridge, K.P., Vorobieff, P., Rightley, P.M., and Benjamin, R.F., Validation of an instability growth model using particle image velocimetry measurements. *Physical Review Letters* **84**, pp. 4353-4356, 2000.
[11] Hecht, J., Alon, U., and Shvarts, D., Potential flow models of Rayleigh-Taylor and Richtmyer-Meshkov bubble-fronts. *Physics of Fluids* **6**, pp. 4019-4030, 1994.
[12] Zhang, Q., and Sohn, S.I., An analytical nonlinear theory of Richtmyer-Meshkov instability. *Physics Letters A* **212**, pp. 149-155, 1996.
[13] Vorobieff,P., Mohamed, N.-G., Tomkins, C., Goodnight, C., Marr-Lyon, M., and Benjamin, R.F., Scaling evolution in shock-induced transition to turbulence. To be published, *Physical Review E*, 2003.
[14] Tomkins, C., Prestridge, K., Rightley, P., Marr-Lyon, M., Vorobieff, P., and Benjamin, R.F., A quantitative study of the interaction of two Richtmyer-Meshkov-unstable gas cylinders. *Physics of Fluids* **15**, pp. 986-1004, 2003.

Advances in Fluid Mechanics V, A. Mendes, M. Rahman & C. A. Brebbia (Editors)